

# Electromagnetic Radiation from High-Energy Nuclear Collisions

Charles Gale

**Abstract** We highlight some of the developments in the theory and the observation of the electromagnetic radiation, thermal and otherwise, emitted in relativistic heavy-ion collisions.

## 1 Introduction

*Mama always told me not to look into the eyes of the sun  
But mama, that's where the fun is*

-Bruce Springsteen, *Blinded By The Light*

This article is meant, in the spirit of this volume, as a chronicle of the remarkable progress accomplished in the theory and in the measurement of electromagnetic radiation emitted from heavy-ion collisions.

The detection of the electromagnetic radiation emanating from the collision of strongly interacting particles dates back to the very early scattering experiments and even predates the establishment of the theory of the nuclear strong interaction, QCD. Owing to the relative weakness of the electromagnetic coupling,  $\alpha_{EM}/\alpha_s \ll 1$ , photons (real and virtual) offered the promise of a clean probe of the reaction dynamics as the mean free paths associated with the electromagnetic interaction exceed typical hadronic length scales. In the modern era ushered by the availability of high energy hadronic beams, the immense potential of electromagnetic observables became clear, and their status as natural complements to measurements of hadrons was confidently established. To make the discussion specific, the photon production cross section in proton-proton collisions, for example, is calculable in perturbative

---

Charles Gale

Department of Physics, McGill University, 3600 University street, Montreal QC, Canada H3A 2T8  
e-mail: charles.gale@mcgill.ca

QCD (pQCD), with the help of factorization [1]. Consequently, early measurements of electromagnetic radiation at CERN (ISR) and at Fermilab were crucial in the confirmation of the parton model, of QCD itself, and of its perturbative treatment [2,3].

To repeat, the basic feature which makes real and virtual photons so appealing in studies of QCD is that they suffer no final state interactions and decouple from the strongly interacting system. They are therefore good probes of the conditions local to their production site, assuming their formation is under theoretical control. This is also the reason why electromagnetic measurements have accompanied the development of the field now known as relativistic heavy-ion collisions, which concerns itself with the formation, study, and characterization of the quark-gluon plasma, an exotic state of the fundamental constituents of QCD and which is also the central theme of the present volume.

Our current understanding of global heavy-ion reaction dynamics is illustrated in Fig. 1 which shows the different eras which exist in those high-energy scattering events. The need to theoretically address strongly interacting matter over large scales of length and time has driven the development of the multistage approaches currently used to model the evolving system. In heavy-ion collisions, real and virtual photons – the latter will decay into lepton pairs – will be produced at all the different stages of the collision process: this signal can therefore serve to validate multistage models that have been tuned to a variety of hadronic observables as well as act as a tomographic probe of the system. Relativistic heavy-ion physics can rightly claim to be a strong proponent of multimessenger science.

In the rest of this paper, we discuss the techniques needed and used to calculate the generation of electromagnetic radiation from hadronic collisions, concentrating on signals that are thermal and thermal-like.

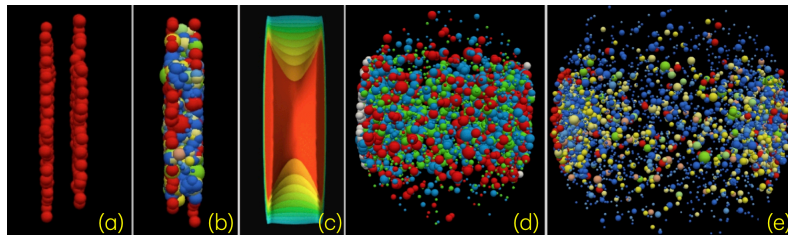


**Fig. 1** The many stages of a heavy-ion collision: (a) Initial state; (b) pre-hydro phase; (c) fluid dynamical evolution; (d) Hadronization; (e) Final-state hadrons eventually free-streaming to the detectors. These images are not from a single end-to-end calculation, but are simply meant to illustrate the different stages. The pictures have been assembled and collected from different sources which include hydrodynamical simulations [4] and UrQMD calculations [5].

## 2 Electromagnetic radiation from systems in equilibrium

As photons leave the reaction site unscathed, they potentially carry pristine information about the local conditions at their creation site. For example, high energy photons can report on the early instants of the collision, an era hardly accessible to hadronic signals, with the possible exception of QCD jets and of heavy quarks. Both of those however undergo in-medium final state interactions.

Some of the early exploratory calculations have been devoted to estimates of the temperature of the quark-gluon plasma, and have proposed measuring the spectrum of lepton pairs with invariant masses  $1 < M \lesssim 3.5$  GeV, and read an effective temperature from its slope in analogy with black body radiation [6–9]. This basic philosophy – using electromagnetic radiation to characterize the QGP – is followed to this day, but with some of the additional sophistication described in this paper.

In a strongly interacting medium at temperature  $T = 1/\beta$ , a starting point to the computation of thermal electromagnetic emission rates is the transition rate between two states, an initial state  $i$  and a final state  $f$ , which can be written as  $R_{fi} = \frac{|S_{fi}|^2}{\tau V}$  with  $\tau V$  being the proper four-volume. To leading order in the electromagnetic interaction, the interaction matrix element written in terms of the electromagnetic current  $J^\mu$  and the photon field  $A^\mu$  is  $S_{fi} = \langle f | \int d^4x J^\mu(x) A_\mu(x) | i \rangle$ . A by now standard set of manipulations [10–14] lead to the expressions for the differential emission rate  $R$  (electromagnetic quanta per unit four-volume) of photons and dileptons:

$$\begin{aligned} \omega \frac{dR_\gamma}{d^4k} &= -\frac{g^{\mu\nu}}{(2\pi)^3} \text{Im} \Pi_{\mu\nu}(\omega, \mathbf{k}) \frac{1}{e^{\beta\omega} - 1} \quad (\text{photons}) \\ E_+ E_- \frac{dR_{\ell\bar{\ell}}}{d^3p_+ d^3p_-} &= \frac{2e^2}{(2\pi)^6} \frac{1}{k^4} L^{\mu\nu} \text{Im} \Pi_{\mu\nu}(\omega, \mathbf{k}) \frac{1}{e^{\beta\omega} - 1} \quad (\text{dileptons}) \end{aligned} \quad (1)$$

The lepton tensor is (for leptons with rest mass  $m_\ell$ )  $L^{\mu\nu} = p_+^\mu p_-^\nu + p_+^\nu p_-^\mu - g^{\mu\nu} (p_+ \cdot p_- + m_\ell^2)$ . The photon (dilepton) four-momentum  $k^\mu = (\omega, \mathbf{k})$  is light-like for real photons and timelike for dileptons. In these equations,  $\Pi^{\mu\nu}$  is the finite-temperature retarded in-medium photon self-energy. Importantly, these equations are valid up to first order in the electromagnetic coupling, but are *exact* in the strong coupling [13]. This formalism is then directly amenable to non-perturbative field theoretical calculations, where the photon self-energy can be written as a two-point correlator of the electromagnetic current [13] obtainable by analytically continuing the Euclidean correlator evaluated non-perturbatively on the lattice. For a non-Abelian gauge theory like QCD this is a technically challenging procedure [15, 16], but recent progress has been reported [17].

An alternative approach to the evaluation of electromagnetic radiation production rates is provided by the fact that taking the imaginary part of the photon self-energy is tantamount to putting internal virtual particles on-shell, enabling in principle a formalism based on kinetic theory [11, 18, 19]. In this language, the photon production rate from the reaction  $1 + 2 \rightarrow 3 + \gamma$  is

$$R_\gamma = \mathcal{N} \int \frac{d^3 p_1}{2E_1 (2\pi)^3} \frac{d^3 p_2}{2E_2 (2\pi)^3} f_1(E_1) f_2(E_2) (2\pi)^4 \delta(p_1^\mu + p_2^\mu - p_3^\mu - k^\mu) \\ \times |\mathcal{M}|^2 \frac{d^3 p_3}{2E_3 (2\pi)^3} \frac{d^3 k}{2\omega (2\pi)^3} [1 \pm f_3(E_3)] \quad (2)$$

where  $\mathcal{N}$  is an overall degeneracy factor, the  $f$ 's are Fermi-Dirac or Bose-Einstein distribution functions as appropriate, and the matrix element for this interaction is  $\mathcal{M}$ . Those two approaches have their own advantages and disadvantages, and are often used as being complementary.

The historical development of thermal emission rates from strongly interacting matter as that created in heavy-ion collisions is an interesting story in itself. Calculations of photons and dileptons from the hot QGP involve the interactions between gluons and quarks in a finite-temperature medium. Early kinetic theory calculations provided estimates of photon and dilepton emission from interacting partons [6, 7, 20–22]. Reformulating the production rate of real photons in terms of the photon self-energy with Eq. (1) in mind, the processes at leading order in  $\alpha_s$ :  $qg \rightarrow q\gamma$  and  $q\bar{q} \rightarrow g\gamma$  appear at two loops. If the virtual quarks exchanged in those previous reactions are massless, the emission rate suffers from a logarithmic collinear singularity, cured however by the generation of an in-medium effective fermion mass calculated using the Hard Thermal Loops (HTL) resummation [23, 24]. The formalism of HTL was established earlier and used to famously address the manifest and vexing gauge dependence that plagued calculations of the gluon damping rate in finite temperature QCD<sup>1</sup>.



**Fig. 2** Two photon-producing processes that come from taking the imaginary part of the two-loop photon self-energy. They are (left) bremsstrahlung from a quark (or anti-quark), and (right)  $q\bar{q}$  annihilation with scattering.

Further explorations in the topology of the photon self-energy lead to evaluations of the parton bremsstrahlung contribution to the production of real photons. Using an effective theory based on the resummation of HTLs, this channel enters at the two-loop level, and taking the imaginary parts produces the processes shown in Fig. 2. Even though the naive parametric power counting of the photon self-energy would have those contributions  $\sim g^4$ , where  $g$  is the strong coupling constant, it was

<sup>1</sup> See Refs. [3] in Ref. [25].

found that collinear divergences formally promote the photon rate to  $\sim g^2$  [26]. The solution to the puzzle of how to uncover and sum up all the contributions at a given order of the perturbation expansion was provided with the consistent inclusion of photons generated by the Landau-Pomeranchuk-Migdal effect (LPM), which limits the coherence length of the emitted radiation. The first photon production rates complete at leading order (LO) in the strong coupling were presented in Ref. [27], and results at NLO were reported later in Ref. [28]<sup>2</sup>.

At lower temperatures, the photon rates calculated with the hadronic degrees of freedom relevant to stages (d) and (e) of Fig. 1, were calculated using interactions modeled with effective chiral hadronic Lagrangians in Refs. [23,29–33]. Calculations of dilepton production involving composite hadrons also rely on Eq. (1), but the virtual nature of the photon field reveals the vector meson spectral distribution, owing to the coupling of the photon field with vector meson fields: Vector Meson Dominance [13,34].

It is important to appreciate the perseverance and devotion of the experimental community involved in the measurement of photons and dileptons. Measuring lepton pair production is especially challenging: the rates are smaller than their photon counterpart by a factor of  $\alpha_{\text{EM}}$ , and the analysis requires extraction of the desired signal from a huge combinatorial background.

## 2.1 Electromagnetic emission out of equilibrium

Up to this point in our discussion, the medium emitting photon and dilepton radiation was assumed in equilibrium; thermal and chemical. Those assumptions were also made in most of the early estimates of the electromagnetic emissivity of strongly interacting media. However, the modern understanding of the evolution of relativistic heavy-ion reactions is that the strongly interacting medium is never in total equilibrium in any formal sense. Referring back to Fig. 1, some electromagnetic signal will also be emitted in the stage corresponding to that depicted in (b), and the distinction from a signal coming from a source closer to equilibrium is not possible. Those sources have to be addressed consistently, ideally within a single approach. The theory of radiation emitted out of equilibrium already has a rich history [35,36], but it is also fair to write that a systematic treatment of the pre-hydrodynamics era in relativistic heavy-ion collisions is still being developed. The following is but a summary of some of the recent efforts.

To fix ideas, we first consider the emission of real photons; of course, virtual photons are also emitted out of equilibrium. Before discussing the different models addressing photon emission out of equilibrium and just prior to the hydrodynamics phase, it is instructive to discuss the most extreme case: electromagnetic radiation from the very first nucleon-nucleon collisions. Those photons will appear as an irreducible background to any of the other photon sources under consideration, and

<sup>2</sup> For values of  $\alpha_s$  relevant for the phenomenology discussed here, NLO + LO results show an enhancement of  $\sim 20\%$  over LO, owing to some partial cancellations in the NLO contributions.

will typically occupy the highest  $p_T$  part of the spectrum. As alluded to previously, those are calculable with pQCD, using a procedure that is however not free from uncertainties which grow as  $p_T$  decreases: they are associated with scale uncertainties in the nuclear parton density functions (nPDF) [37–40] and with the relatively poorly known photon fragmentation function (especially from gluons) [41]. This is why the pQCD contributions in the low momentum part  $p_T \approx 1$  GeV/c of the thermal photon window are mostly extrapolations [42] which emphasize the importance of direct measurements of low transverse momentum photons in pp and pA collisions.

Just prior to, but also in the fluid phase, non-equilibrium aspects will manifest themselves in different ways. In the recent couple of decades, the relativistic heavy-ion program pursuing the characterization of the QGP has revealed the remarkable success of viscous fluid dynamical modeling. By comparing with hadronic data, it became apparent that the results of the early calculations based on inviscid hydrodynamics could be brought closer to measurements with the inclusion of transport coefficients such as shear and bulk viscosity [43]; the electromagnetic emissivity evaluations also needed to be adapted consequently.

Deviations from kinetic equilibrium can be obtained by considering the linearized Boltzmann equation and evaluating the deviations ( $\delta f$ ) of the distribution functions ( $f = f_0 + \delta f$ ) from their equilibrium form ( $f_0$ ), using techniques [44] pioneered by Chapman and Enskog [45], and by Grad [46]. Using that approach, the photoproduction channels in the QGP and in the confined hadronic sector involving  $2 \rightarrow 2$  kinematics can be corrected for the presence of shear and bulk viscosity [47] demanded for consistency with the fluid dynamical evolution [48]. The electromagnetic emission rates derived thusly can then be implemented in parallel with the fluid dynamical evolution [42]. Part of this general framework for correcting the photon emission rates is discussed in Ref. [47], and a discussion of the  $2 \rightarrow 2$  photon-producing contributions in the QGP (Compton and quark-anti-quark annihilation) appears in Ref. [49]. To this day not all the photoproduction channels currently include such out-of-equilibrium corrections. In the QGP, this is the case for the photon contribution related to the LPM effect.

It is known that formally, a field-theoretic formulation appropriate for non-equilibrium contributions is based on the real-time formalism as expressed in the “1/2”<sup>3</sup> [50, 51] and “r/a” bases [51]. In that language, the thermal photon spectrum is [52]

$$\omega \frac{dR}{d^3k} = \frac{i}{2(2\pi)^3} \Pi_{12\mu}^\mu, \quad (3)$$

where the photon polarization tensor is no longer the retarded one, but contains the “1” and “2” vertices [51]. Building on this, the effect of the anisotropy in momentum space generated for instance by the presence of a shear pressure tensor  $\pi^{\alpha\beta}$  in photon production in general – including LPM – has been elaborated in Ref. [53], paving the way for a future holistic treatment of out-of-equilibrium effects, even if the presence of early medium instabilities requires some care [54].

<sup>3</sup> The numbers label two branches in the complex time plane [50, 51].

Studies of photon production obtained by solving some form of kinetic transport theory in the partonic phase prior to “hydrodynamization” have also been performed [55–61]. The kinetic theory approaches aim to solve the Boltzmann equation and therefore to also capture the non-equilibrium aspects of the space-time evolution. However, in such simulations the inclusion of the LPM effect – which is due to quantum interference between multiple scatterings – has been more challenging, and has driven the need for different approximations [57, 60, 62].

At least in principle, the non-equilibrium behavior of a collection of partons can be assessed by solving a set of coupled Boltzmann equations which contain all of the relevant scattering processes. In K $\emptyset$ MP $\emptyset$ ST, as introduced and defined in Refs. [63, 64], the kinetic theory of Ref. [65] is used to construct an energy-momentum tensor  $T^{\mu\nu}$  which is coarse-grained and acts as an average background over which fluctuations are propagated using linear response theory. Owing to some robust scaling properties of the Green’s functions used in the linear response regime [63], this alternative approach to the full solutions of the Boltzmann equation offers some practical advantages. With this approach at hand, one can also evaluate the contribution of the non-equilibrium regime to electromagnetic radiation production using a procedure detailed in Ref. [66]. The energy-momentum tensor generated by K $\emptyset$ MP $\emptyset$ ST is decomposed as it is in the hydrodynamics phase, and the energy density, flow velocity, and viscosity contributions are identified. Then, a cell-by-cell effective temperature is extracted at each time step of the dynamical evolution using the QCD equation of state [67]. Even though this procedure is approximate, it enables continuity of the electromagnetic emissivity between the fluid dynamical epoch and that preceding it. In a given practical implementation, the K $\emptyset$ MP $\emptyset$ ST stage is inserted between an IP-Glasma initial state [68] which is itself derived from the Color Glass Condensate picture of high-energy hadronic scattering, and the viscous hydrodynamics evolution [43].

Clearly, the exact chemical composition of the initial state will also influence the radiation of photons, which require some fermions in the initial state. The fermion content in many approaches is evolved dynamically from an initial gluon-dominated many-body wave function. This makes the measurement of photons – both real and virtual – even more interesting as they can report not only on the effective temperature of the medium, but also on its early chemical content.

With all of those aspects in mind and several of them still in flux, it is revealing to compare the spectra of real photons obtained with the non-equilibrium approaches detailed in Refs. [56, 57, 60, 66] and shown in Fig. 3. In each of those calculations, the initial state was treated differently. The AFTm (Abelian Flux Tube model) sets up an initial chromo-electric field which decays and populates the fermion distributions [60]. In PHSD (Parton Hadron String Dynamics) [56] it is string breaking which initializes the partons, which are evolved with the relativistic transport theory. The BAMPS (Boltzmann Approach to Multiparton Scatterings) simulations [57] are based on a gluon-dominated initial state, as does the multistage calculation involving K $\emptyset$ MP $\emptyset$ ST discussed in [66], but the evolution times of the classical Yang-Mills equations are a parameter of the model. In BAMPS, the gluon Wigner distributions are sampled from the solution of the classical Yang-Mills and then propagated in the

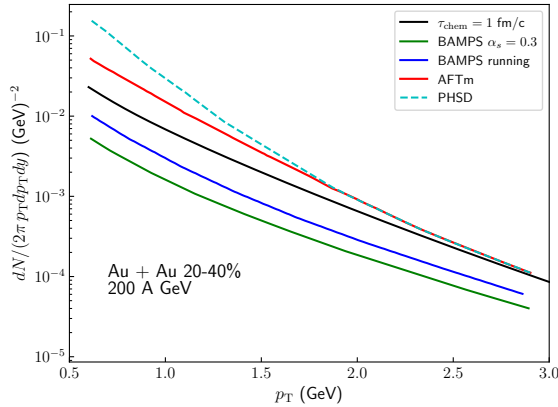


**Fig. 3** The invariant photon spectrum plotted as a function of photon transverse momentum at midrapidity, for conditions corresponding to Au + Au collisions at RHIC, in the 20-40% centrality window. The transport theory results are those obtained with: BAMPS with fixed and running strong interaction coupling; the Abelian Flux Tube model (AFTm); the Parton Hadron String Dynamics (PHSD). The results from those models were adapted from Fig. 8 in [60]. The photon results obtained using KØMPØST, as in Ref. [66], are also shown and labeled  $\tau_{\text{chem}} = 1 \text{ fm}/c$  (see main text).

partonic cascade. In the multistage model the energy-momentum tensor is passed from IP-Glasma to KØMPØST and then fed to the hydrodynamic evolution. Clearly all the approaches discussed so far – those with results highlighted in Fig. 3 – differ in the details of their respective implementation even though some of the basic principles are common.

It is still early to come to a definite picture: the theory of non-equilibrium electromagnetic radiation in heavy-ion collisions has experienced rapid growth in the last few years and features many results in addition to those shown in Fig. 3. This topic is now at the point where more detailed comparisons between models would serve the field well, and new data with reduced uncertainties could also make it possible for some of the model parameters to be incorporated in Bayesian studies to follow those of the current generation [69–71]. In the current state of knowledge and for conditions (system and energy) relevant to RHIC as shown on the figure, the different model assumptions generate non-equilibrium photon spectra which can easily differ by an order of magnitude for low  $p_T \approx 1 \text{ GeV}$ , and roughly half that at  $p_T \approx 3 \text{ GeV}$ . It is therefore important to compare the pre-equilibrium signal to that generated from other stages of the collision, and with the available data.



## 2.2 Net photon yields

In heavy-ion collisions, direct real photons have been measured by several collaborations; in the context of the search for the quark gluon plasma (QGP) earlier measurements were conducted by WA93 [72] and WA98 [73] at the CERN SPS, followed by STAR [74] and PHENIX [75] at the Relativistic Heavy-Ion Collider (RHIC), and by ALICE [76] at the Large Hadron Collider (LHC). We concentrate on data from RHIC and the LHC and will show results obtained with the multistage approach of Ref. [66], which begins with IP-Glasma followed by K $\phi$ MP $\phi$ ST and then viscous fluid dynamics. The late hadronic state corresponding to a combination of the phases (d) and (e) of Fig. 1 of course also emits real and virtual photons (*e.g.*  $\pi\rho \rightarrow \pi\gamma$ , etc) [66, 77]. These next results are obtained using all the currently available direct photon rates integrated with a relativistic viscous fluid dynamical calculation tuned to reproduce hadronic data.

Figure 4 displays direct photon yields<sup>4</sup> and contains data gathered by the PHENIX and STAR collaborations in collisions of Au + Au at 200 A GeV, at RHIC, and by the ALICE collaboration in collisions of Pb + Pb at 2760 A GeV at the LHC. The parameter  $\tau_{\text{chem}}$  is a chemical relaxation time, and its significance and value are discussed in Ref. [66]. The sum of direct real photons (long dashes) is further

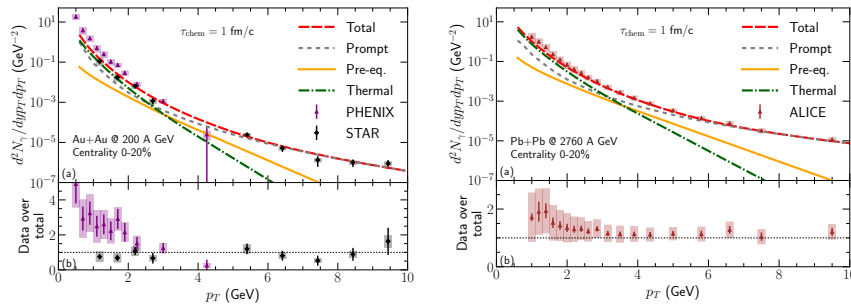


**Fig. 4** The yield distribution (top panels) of real photons shown with the appropriate experimental data measured in a 0–20% centrality window. The contributions of the different processes discussed in the text are shown separately. (Left panel) Photons from Au + Au collisions at 200 A GeV. The data are from the PHENIX [78] and STAR [79] Collaborations. (Right panel) Photons from Pb + Pb collisions at 2760 A GeV. The data are from the ALICE Collaboration [80]. The bottom panels show the ratio of data over the calculated result. Figure adapted from [66].

decomposed into channels which include: photons from the first-impact collisions calculated with pQCD (“prompt”, short dashes); pre-hydrodynamics photons (“pre-equilibrium”, solid); thermal photons from the QGP and from the ensemble of composite hadrons (dot-dash). One observes that at RHIC, the pre-equilibrium, thermal, and pQCD photon contributions are comparable at  $p_T \approx 3$  GeV, and at the

<sup>4</sup> The photons from decays of hadrons are measured and subtracted in order to obtain the direct signal.

LHC, for  $p_T \approx 3.5$  GeV: the pre-equilibrium contribution represents  $\gtrsim 30\%$  of the net photon yield and thus has a promising future as an observable signal. At the LHC energy shown in Fig. 4, the model and data agree within statistical uncertainties. Note in passing the unfortunate and enduring disparity between PHENIX and STAR results [81].

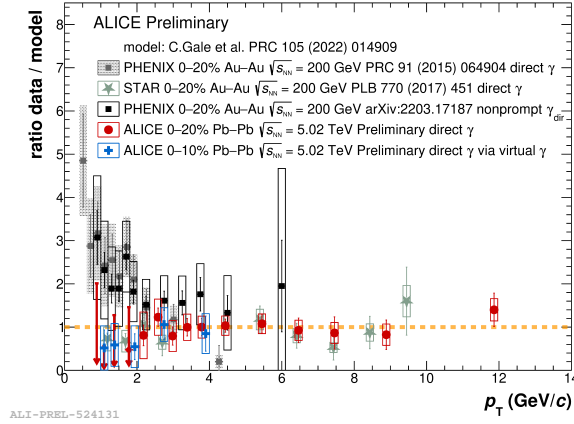


**Fig. 5** The direct photon transverse momentum spectrum measured by the PHENIX, STAR, and ALICE Collaborations, divided by the calculations of [66]. The figure is from Ref. [82] (Creative Common License, CC-BY 4.0).

More recently, the ALICE Collaboration has released data on real direct photons emitted in collisions of Pb + Pb at  $\sqrt{s_{NN}} = 5.02$  TeV analyzed with different methods (photon conversion and virtual photon) [82]. Fig. 5 shows those data, together with previous data from the PHENIX and STAR Collaborations at RHIC divided by results of the calculation discussed earlier which also made predictions for the eventual 5.02 TeV measurements [66]. The new data and the model predictions are in agreement within statistical uncertainties.

### 2.3 Net photon flow

As is the case for hadrons, the measurement of the anisotropy of photon momentum distributions contains valuable information about the microscopic dynamics of the processes participating in photon production [83]. Because of limited statistics, the measurement and calculation of photon flow – or photon momentum anisotropy – do not proceed via photon-photon correlations (unlike hadrons), but utilize photon-hadron correlations:

$$v_n(p_T^\gamma) = \frac{\langle v_n^\gamma(p_T^\gamma) v_n^h \cos(n [\Psi_n^\gamma(p_T^\gamma) - \Psi_n^h]) \rangle}{\sqrt{\langle (v_n^h)^2 \rangle}} \quad (4)$$

In the equation above,  $v_n^\gamma$  is the photon flow coefficient,  $v_n^h$  is that of charged hadrons, and  $\Psi_n^i$  is the event plane angle of photons ( $i = \gamma$ ) and hadrons ( $i = h$ ). The hadrons are used to define a reference plane, and the photon momentum anisotropy is measured with respect to this plane [42]. Therefore, prior to the consideration of electromagnetic observables and of their momentum anisotropy, it is imperative that the hadronic sector of any calculation be in agreement with the corresponding data.

Figure 6 shows the results of calculating photon elliptic flow,  $v_2(p_T^\gamma)$ , with the multistage model, at RHIC and at LHC energies. The message is that the photon flow measured by the PHENIX Collaboration is underestimated by the model. The same can be said for the photon flow measured at the LHC, but the statistical significance of the deviation is considerably less. A similar difference between theory and data

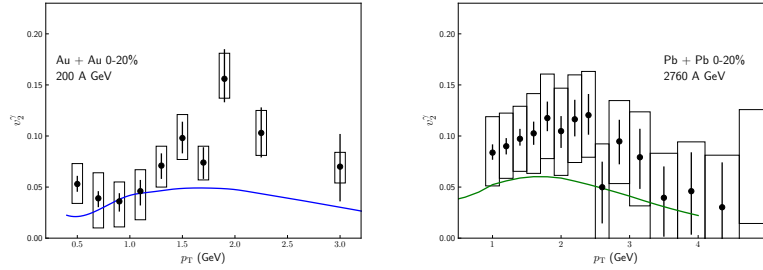


**Fig. 6** (Left panel) The direct photon elliptic flow coefficient,  $v_2^\gamma(p_T)$ , for collisions of Au + Au at an energy of 200 A GeV, at midrapidity. The data are measured by the PHENIX Collaboration using the conversion method [84]. The error bars correspond to statistical uncertainties, and the boxes represent systematic uncertainties. (Right panel) The direct photon  $v_2^\gamma(p_T)$  measured by the ALICE Collaboration for Pb + Pb collisions at 2760 A GeV [85]. The error bars are statistical uncertainties and the boxes, the total uncertainty. In both panels the curve is the result of calculations with the approach described in Ref. [66], with  $\tau_{\text{chem}} = 1$  fm/c as shown previously.

(especially at RHIC) is observed in other calculations using modeling based on either fluid dynamics, thermal fireballs [86], or PHSD [56]. The tension between data and calculation for the combined photon spectrum and  $v_2$  has been termed the “direct photon puzzle”; a clear solution has yet to be identified [81].

The direct photon puzzle has driven the development of some new research ideas, while bringing theory and experiments under increased scrutiny [81]. For instance, it has triggered the re-examination of some previous estimates of photon emission around the cross-over temperature from partonic to composite hadronic matter [86–88]. Among the topics put forward to possibly address the puzzle is the effect on electromagnetic radiation of the early strong magnetic fields<sup>5</sup> generated

<sup>5</sup>  $B \approx 10^{18} G$ , the strongest known in Nature [89–92]

in non-central heavy ion collisions [93–98]. The cumulative effect of including all known corrections to the photon yield and flow coefficients is still to be worked out, however it is likely that knowing the global effect of strong electromagnetic fields on all observables will likely have to wait for the development of relativistic magneto-hydrodynamics as applied to heavy-ion collisions [99, 100].

## 2.4 Dileptons

The evolution of thermal rates for dilepton emission [101–104] has proceeded in parallel with that of real photons, and the effect of viscosity corrections has been discussed and highlighted there as well [105–107]. As was the case for the emission of real photons, not all channels have been corrected for viscous effects. For example, low invariant mass ( $M < m_\phi$ ) lepton pairs will receive a large contributions from baryons affecting  $\Pi_{\mu\nu}$  in Eq. (1) [108]; estimates of viscous effects there are still being performed. In the QGP, the electromagnetic emissivity of an ensemble of hot partons is known today at NLO, and at finite baryon density,  $\mu_B \neq 0$  [109]. Note that photon rates complete at  $O(\alpha_s)$ ,  $\mu_B \neq 0$ , and including the LPM effect had been established in Ref. [110]. Both of those will be treated in the future for non-equilibrium effects owing to viscosity.

The dilepton-equivalent of the “cold photons” calculable in pQCD, are those originating from the Drell-Yan (DY) process [2]. The calculations of DY cross sections have also been integrated in numerical packages such as Pythia [111], or the more specialized DYTurbo [112] which performs a transverse-momentum resummation up to next-to-next-to-leading logarithmic accuracy, combined with fixed-order results at next-to-next-to-leading order (NNLO). Those two permit the evaluation of the irreducible background to a thermal dilepton signal.

Even though the thermal dilepton yield stems from the same current-current correlator as for the real photons, measurements of dileptons offer in addition the potential to reveal the status of chiral symmetry restoration, as mentioned previously, as well as the hope to access an in-medium temperature that is impervious to kinematic distortions. The “dilepton thermometer” exists because the yield of lepton pairs can be calculated and measured as a function of their invariant mass  $M^2 = (p_+ + p_-)^\mu (p_+ + p_-)_\mu$ , whereas real photons are confined to the light cone and their spectrum depends on their momentum which is not a Lorentz invariant. For instance, photon spectra will experience Doppler shift: the local motion in the lab frame of a given cell will distort the fluid rest frame photon distribution. This makes photon and dilepton measurements *complementary*: in addition to the effective temperature information, the photon spectra will also inform the fluid dynamical modeling [113–115], while the dilepton spectra will offer a Doppler-free reading. Note however that measurements will still consist of lepton pairs emitted at all stages of Fig. 1, and over a distribution of cell temperatures.

In terms of measurements, low and intermediate mass dileptons were previously analyzed by the pioneering DLS experiment [116] at the LBNL Bevalac, and at the

CERN SPS by the CERES NA38/NA50, and Helios-3 Collaborations [117]. In the low invariant mass region (LMR),  $M \lesssim 1$  GeV, the dilepton spectrum measured with great precision by the NA60 Collaboration in collisions of In + In at A 158 GeV reveals [118] a striking broadening of the  $\rho$  meson spectral density, where coupling with baryon resonances plays a decisive role [34]. At RHIC, dileptons are investigated by the STAR [119] and PHENIX [120] Collaborations, and at the LHC by ALICE [121]. For the collider conditions prevailing at RHIC, the STAR collaboration has reported dilepton measurements at various energies, namely BES-I and -II (Beam Energy Scan) and  $\sqrt{s_{NN}} = 200$  GeV. The LMR measurements agree [122] with calculations based on the same spectral density integrated with a thermal fireball model previously found to match the one extracted by NA60 from the In + In data [123], also supporting the scenario where  $\rho$  meson broadening is driven by interaction with baryon resonances.

The dilepton spectrum in the intermediate mass region (IMR),  $1 \text{ GeV} < M \lesssim 3$  GeV has been the focus of some attention because of the possibility for dilepton measurements to reveal a possible restoration of chiral symmetry in a hot and dense strongly interacting system [34], proceeding through a mixing of the vector and axial-vector spectral densities [124]. This would however necessitate the observation of the pseudovector spectral density [124–126], which has however remained elusive. Because a clear signal of this restoration is still ambiguous, the NA60+ Collaboration has put forward a new experiment proposal which features the search for chiral symmetry restoration effects through  $\rho - a_1$  mixing, the study of the order of the phase transition at large baryochemical potential through the measurement of a caloric curve, and the onset of the deconfinement through the measurement of  $J/\Psi$  suppression at the CERN SPS. The letter of intent [127] states that chiral restoration would generate a 20-25% enhancement of the dilepton invariant mass spectrum over the case where the  $\rho$  and the  $a_1$  do not mix, around  $M \sim 1$  GeV. If approved, data taking could start in 2029.

We leave the observation of chiral symmetry restoration as a tantalizing possibility for now and concentrate on temperature extractions, which has been the subject of previous phenomenological and experimental studies [118, 128, 129]. Recent analyses done using the multistage approach introduced earlier have also been completed [109, 130]. The first lesson from these recent papers is the importance of next-to-leading order (in the strong coupling) QCD contributions to the dilepton spectrum coming from the hot partonic medium, when compared to results obtained at leading order (LO). This is made clear in Fig. 7 which shows the thermal lepton pair production rate  $\Gamma$  (@LO and @NLO) as a function of invariant mass for different medium temperatures. Clearly, NLO corrections have a considerable effect – qualitatively and quantitatively, depending on the temperature – at low ( $M < 1$  GeV) invariant mass, but also affect the intermediate mass ( $1 \text{ GeV} \lesssim M \lesssim 3$  GeV) region. Note that the need to go beyond the Born term for dilepton production at finite temperature had been known for some time [25, 131]. In the future, as was the case for some channels contributing to real photon emission, NLO dilepton emission rates will have to be corrected for non-equilibrium conditions; some of this has been done for LO rates [105–107, 132].

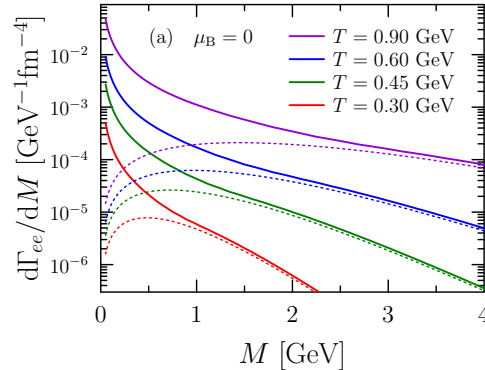


**Fig. 7** Thermal dilepton emission rates for a static midrapidity source with vanishing net baryon density at different temperatures, as a function of the dilepton invariant mass  $M$ . The dotted lines represent the emission rate computed at leading order (LO) in the strong coupling ( $O(\alpha_s^0)$ ), and the solid curves are the emission rates at full NLO ( $O(\alpha_s)$ ). This figure is adapted from [109].

The emission of lepton pairs from the pre-hydro era had received some attention [133]. Recent estimates based on using either kinetic theory or K $\phi$ MP $\phi$ ST (as was done for photons) and including the contribution of the Drell-Yan lepton pairs have been completed [134–136], and the pre-equilibrium dilepton spectra computed for LHC conditions in those two approaches have been found to have very similar characteristics [137]. The conclusion that follows from those studies is that a pre-equilibrium component can contribute measurably to the spectrum of dileptons in the intermediate mass region, at an LHC energy (5.02 TeV). Those dileptons will outshine those from the Drell-Yan process and the clarity of this signal will greatly benefit from the explicit measurement of lepton pairs coming from the simultaneous decay of open charm mesons, as planned by the next generation of experiments.

Finally, the dilepton spectrum can be formulated as a double differential, where the  $p_T$  spectrum can be studied in various windows of invariant mass, for instance. This additional feature which is absent for real photons will constitute a demand on experimental statistics, but can highlight further dynamical effects, like the chemical equilibrium at early times [136] or the value of QCD transport parameters [105].

Considering the evolution in the calculation of emission rates and the current sophistication of the multistage modeling approaches, a legitimate question to ask is whether the promise of the early – possibly optimistic – estimates [7] of extracting legitimate temperatures from the slope of the dilepton spectrum measured in heavy-ion collisions can be realized, many decades later. A recent study was devoted specifically to this question [130], where values of temperature extracted from the slope of dilepton spectra in the intermediate mass region calculated at NLO in QCD at finite temperature and non-zero baryon chemical potential were compared with values of “true” temperature found within the (3+1)D relativistic viscous hydrody-

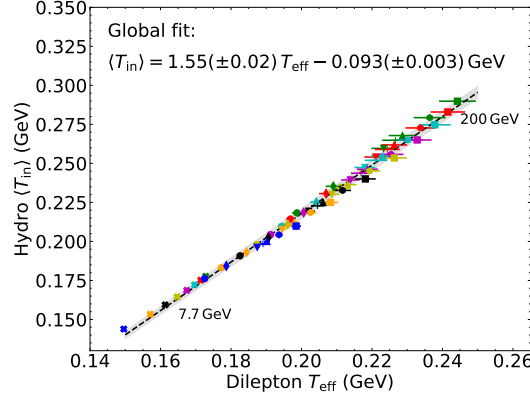


**Fig. 8** Correlation between the average initial temperature  $\langle T_{in} \rangle$  of the fluid dynamical model and the effective temperature obtained from the slope of the dilepton spectrum in the intermediate mass region. The plot contains several regions of centrality, and energies from 7.7 to 200 GeV. The black dashed line is a global fit to all data points and the gray band represents the uncertainty related to the fitting procedure. This figure is adapted from Ref. [130].

namics simulations. The summary of this study is found in Fig. 8, which shows a clear correlation between the average initial hydrodynamical temperature  $\langle T_{in} \rangle$  and  $T_{eff}$ , the temperature extracted from dilepton spectra produced in Au + Au collisions spanning a range of centralities and energies from 7.7 to 200 GeV. The correlation between “effective” and “true” temperatures is much tighter than when analyzed with photons [114]. The figure highlights a linear correlation, even though the average initial temperature  $\langle T_{in} \rangle$  is really the central value of some broad distribution [130] over several fluid cells. It is exciting to note that almost all of the extracted values of temperature lie above the pseudo-critical value  $T_{pc} \approx 156$  MeV, at  $\mu_B = 0$  extracted from lattice QCD [138]. The results shown in Fig. 8 also drive home the point that even something as physical as temperature will need a realistic theoretical model tuned to other data (hadronic and otherwise) to be interpreted properly.

Finally, the flow coefficients ( $v_n(p_T)$ ) of dileptons also contain previous information, in particular since their spectrum is in principle a function of invariant mass and transverse momentum [105–107, 132, 139]. Preliminary flow measurements have been reported [140] by the STAR Collaboration at RHIC.

Another aspect of electromagnetic signals from heavy-ion collisions that has yet to receive more attention is that of polarization. For heavy-ion collisions at lower energies than those studied at RHIC and at the LHC – those at SIS and at the CERN SPS – the angular lepton distributions reflecting the virtual photon polarization have been studied [141, 142] using coarse-grained transport models, and have been measured by the NA60 [143] and HADES [142] Collaborations. At those energies, the angular distribution of low invariant-mass dileptons is consistent with the presence of the resonances generated by the interactions of the composite hadrons, with little or no apparent sign of a QGP signal. In collider conditions,

the polarization of the virtual photons produced in quark-antiquark annihilation at leading order has been studied in theory and used as a probe of the QGP momentum anisotropy [144, 145], and so has that of real photons [146].

However, as was the case for the dilepton mass spectra, polarization studies of the QGP demand NLO corrections in the low and intermediate invariant mass regions: as  $M \rightarrow 0$ , the LO Born term  $q\bar{q} \rightarrow \gamma^*$  has no phase space to produce a real photon. This is illustrated in the following: the virtual photon polarization can be observed via the angular distribution of final-state leptons in a given Lorentz frame. In the rest frame of the virtual photon, the helicity frame, the coefficient of the polar angle distribution of one of the lepton in the dilepton is  $\lambda_\theta$  and can be shown to be related<sup>6</sup> to the transverse (T) and longitudinal (L) components of the dilepton spectral density [147]:  $\lambda_\theta \sim (\rho_T - \rho_L) / (\rho_T + \rho_L)$ . There again, one observes stark qualitative and quantitative differences between  $\lambda_\theta^{\text{LO}}$  and  $\lambda_\theta^{\text{NLO}}$ . One can show that  $\lim_{M \rightarrow 0} \lambda_\theta^{\text{NLO}} = 1$ , because  $\lim_{M \rightarrow 0} \rho_L^{\text{NLO}} = 0$ , as expected of a real photon. On the other hand,  $\lim_{M \rightarrow 0} \lambda_\theta^{\text{LO}} \neq 1$  [147]. Finally, it is encouraging to note that, after properly averaging  $\lambda_\theta$  over hydrodynamical fluid cells using a realistic space-time model, the characteristic profile survives the fluid evolution [147]: clearly, electromagnetic polarization is another precious variable to signal the presence of a QGP.

### 3 Conclusions

It is evident that during the last five decades, the progress in theory and measurement of electromagnetic radiation emitted in relativistic heavy-ion collisions has been remarkable. This owes much to the advances in treating the electromagnetic emissivity in its own right, but this progress was realized concurrently with rapid developments in the modeling of relativistic nuclear collisions. It is exciting that a clear thermal signal has been seen in the data; its quantification requires accompanying theoretical modeling but the models have grown tremendously in maturity. Photons and dileptons can act as tomographic probes which can also inform our understanding of the space-time evolution of the interaction volume. This is indeed the era of multimessenger heavy-ion physics. What remains to be done in theory is integrating the many aspects we have seen in the paper into an end-to-end approach. This is not a small task but the roadmap is clear and if recent developments are any indication, its realization is within reach.

There are several aspects of the emission of electromagnetic in heavy-ion collisions that this article could not cover. A few examples are that of electromagnetic interferometry [148, 149], of real and virtual photon emission from small systems [150], of radiation from jet-medium interactions [151, 152], and the radiation of photons with very low momenta [153]. Clearly, the study of electro-

---

<sup>6</sup> In a static medium, for lepton and antilepton with negligible rest mass.



magnetic emission from nuclear collisions is a rich and still evolving topic which is perhaps now entering its golden age.

**Acknowledgements** I am happy to acknowledge many collaborators over the years spent on this topic. I am also grateful for valuable comments from Han Gao, Greg Jackson, Jean-François Paquet, Björn Schenke, and Xiang-Yu Wu. This work was funded in part by the Natural Sciences and Engineering Research Council of Canada (NSERC) [SAPIN-2020-00048].

## References

1. R.D. Field, *Applications of perturbative QCD*. Frontiers in physics ; v. 77 (Addison-Wesley, Reading, Mass, 1989)
2. S.D. Drell, T.M. Yan, Phys. Rev. Lett. **25**, 316 (1970). DOI 10.1103/PhysRevLett.25.316. [Erratum: Phys.Rev.Lett. 25, 902 (1970)]
3. J.F. Owens, Rev. Mod. Phys. **59**, 465 (1987). DOI 10.1103/RevModPhys.59.465
4. B. Schenke, S. Jeon, C. Gale, Phys. Rev. C **82**, 014903 (2010). DOI 10.1103/PhysRevC.82.014903
5. M. Bleicher, et al., J. Phys. G **25**, 1859 (1999). DOI 10.1088/0954-3899/25/9/308
6. E.V. Shuryak, Phys. Lett. B **78**, 150 (1978). DOI 10.1016/0370-2693(78)90370-2
7. K. Kajantie, H.I. Miettinen, Z. Phys. C **9**, 341 (1981). DOI 10.1007/BF01548770
8. G. Domokos, J.I. Goldman, Phys. Rev. D **23**, 203 (1981). DOI 10.1103/PhysRevD.23.203
9. K. Kajantie, J.I. Kapusta, L.D. McLerran, A. Mekjian, Phys. Rev. D **34**, 2746 (1986). DOI 10.1103/PhysRevD.34.2746
10. E.L. Feinberg, Nuovo Cim. A **34**, 391 (1976)
11. L.D. McLerran, T. Toimela, Phys. Rev. D **31**, 545 (1985). DOI 10.1103/PhysRevD.31.545
12. H.A. Weldon, Phys. Rev. D **42**, 2384 (1990). DOI 10.1103/PhysRevD.42.2384
13. C. Gale, J.I. Kapusta, Nucl. Phys. B **357**, 65 (1991). DOI 10.1016/0550-3213(91)90459-B
14. J.I. Kapusta, C. Gale, *Finite-Temperature Field Theory : Principles and Applications, 2nd edition* (Cambridge University Press, 2007). DOI 10.1017/9781009401968
15. J. Ghiglieri, O. Kaczmarek, M. Laine, F. Meyer, Phys. Rev. D **94**(1), 016005 (2016). DOI 10.1103/PhysRevD.94.016005
16. M. Cè, T. Harris, A. Krasniqi, H.B. Meyer, C. Török, Phys. Rev. D **106**(5), 054501 (2022). DOI 10.1103/PhysRevD.106.054501
17. S. Ali, D. Bala, A. Francis, G. Jackson, O. Kaczmarek, J. Turnwald, T. Ueding, N. Wink, Phys. Rev. D **110**(5), 054518 (2024). DOI 10.1103/PhysRevD.110.054518
18. H.A. Weldon, Phys. Rev. D **28**, 2007 (1983). DOI 10.1103/PhysRevD.28.2007
19. A. Majumder, C. Gale, Phys. Rev. C **65**, 055203 (2002). DOI 10.1103/PhysRevC.65.055203
20. B. Sinha, Phys. Lett. B **128**, 91 (1983). DOI 10.1016/0370-2693(83)90080-1
21. R.C. Hwa, K. Kajantie, Phys. Rev. D **32**, 1109 (1985). DOI 10.1103/PhysRevD.32.1109
22. G. Staadt, W. Greiner, J. Rafelski, Phys. Rev. D **33**, 66 (1986). DOI 10.1103/PhysRevD.33.66
23. J.I. Kapusta, P. Lichard, D. Seibert, Phys. Rev. D **44**, 2774 (1991). DOI 10.1103/PhysRevD.44.2774. [Erratum: Phys.Rev.D 47, 4171 (1993)]
24. R. Baier, H. Nakkagawa, A. Niegawa, K. Redlich, Z. Phys. C **53**, 433 (1992). DOI 10.1007/BF01625902
25. E. Braaten, R.D. Pisarski, Nucl. Phys. B **337**, 569 (1990). DOI 10.1016/0550-3213(90)90508-B
26. P. Aurenche, F. Gelis, R. Kobes, H. Zaraket, Phys. Rev. D **58**, 085003 (1998). DOI 10.1103/PhysRevD.58.085003
27. P.B. Arnold, G.D. Moore, L.G. Yaffe, JHEP **12**, 009 (2001). DOI 10.1088/1126-6708/2001/12/009

28. J. Ghiglieri, J. Hong, A. Kurkela, E. Lu, G.D. Moore, D. Teaney, *JHEP* **05**, 010 (2013). DOI 10.1007/JHEP05(2013)010
29. U.G. Meissner, *Phys. Rept.* **161**, 213 (1988). DOI 10.1016/0370-1573(88)90090-7
30. C. Song, *Phys. Rev. C* **47**, 2861 (1993). DOI 10.1103/PhysRevC.47.2861
31. S. Turbide, R. Rapp, C. Gale, *Phys. Rev. C* **69**, 014903 (2004). DOI 10.1103/PhysRevC.69.014903
32. M. Heffernan, P. Hohler, R. Rapp, *Phys. Rev. C* **91**(2), 027902 (2015). DOI 10.1103/PhysRevC.91.027902
33. N.P.M. Holt, P.M. Hohler, R. Rapp, *Nucl. Phys. A* **945**, 1 (2016). DOI 10.1016/j.nuclphysa.2015.09.008
34. R. Rapp, *J. Wambach, Adv. Nucl. Phys.* **25**, 1 (2000)
35. F. Michler, H. van Hees, D.D. Dietrich, S. Leupold, C. Greiner, *Annals Phys.* **336**, 331 (2013). DOI 10.1016/j.aop.2013.05.021
36. B. Schenke, C. Greiner, *Phys. Rev. C* **73**, 034909 (2006). DOI 10.1103/PhysRevC.73.034909
37. P. Aurenche, M. Fontannaz, J.P. Guillet, E. Pilon, M. Werlen, *Phys. Rev. D* **73**, 094007 (2006). DOI 10.1103/PhysRevD.73.094007
38. F. Arleo, K.J. Eskola, H. Paukkunen, C.A. Salgado, *JHEP* **04**, 055 (2011). DOI 10.1007/JHEP04(2011)055
39. M. Klasen, C. Klein-Bösing, F. König, J.P. Wessels, *JHEP* **10**, 119 (2013). DOI 10.1007/JHEP10(2013)119
40. P. Paakkinen, *Frascati Phys. Ser.* pp. 33–40 (2017)
41. M. Klasen, F. König, *Eur. Phys. J. C* **74**(8), 3009 (2014). DOI 10.1140/epjc/s10052-014-3009-x
42. J.F. Paquet, C. Shen, G.S. Denicol, M. Luzum, B. Schenke, S. Jeon, C. Gale, *Phys. Rev. C* **93**(4), 044906 (2016). DOI 10.1103/PhysRevC.93.044906
43. C. Gale, S. Jeon, B. Schenke, *Int. J. Mod. Phys. A* **28**, 1340011 (2013). DOI 10.1142/S0217751X13400113
44. G.S. Denicol, D.H. Rischke, *Microscopic foundations of relativistic fluid dynamics* (Springer, 2022)
45. S. Chapman, T.G. Cowling, *The mathematical theory of non-uniform gases: an account of the kinetic theory of viscosity, thermal conduction and diffusion in gases* (Cambridge university press, 1990)
46. H. Grad, *Communications on pure and applied mathematics* **2**(4), 331 (1949)
47. M. Dion, J.F. Paquet, B. Schenke, C. Young, S. Jeon, C. Gale, *Phys. Rev. C* **84**, 064901 (2011). DOI 10.1103/PhysRevC.84.064901
48. U. Heinz and B. Schenke, this volume
49. C. Shen, J.F. Paquet, U. Heinz, C. Gale, *Phys. Rev. C* **91**(1), 014908 (2015). DOI 10.1103/PhysRevC.91.014908
50. J. Schwinger, *Journal of Mathematical Physics* **2**(3), 407 (1961). DOI 10.1063/1.1703727. URL <https://doi.org/10.1063/1.1703727>
51. L.V. Keldysh, *Zh. Eksp. Teor. Fiz.* **47**, 1515 (1964)
52. J. Serreau, *JHEP* **05**, 078 (2004). DOI 10.1088/1126-6708/2004/05/078
53. S. Hauksson, S. Jeon, C. Gale, *Phys. Rev. C* **97**(1), 014901 (2018). DOI 10.1103/PhysRevC.97.014901
54. S. Hauksson, S. Jeon, C. Gale, *Phys. Rev. C* **103**, 064904 (2021). DOI 10.1103/PhysRevC.103.064904
55. M. Chiu, T.K. Hemmick, V. Khachatryan, A. Leonidov, J. Liao, L. McLerran, *Nucl. Phys. A* **900**, 16 (2013). DOI 10.1016/j.nuclphysa.2013.01.014
56. O. Linnyk, V. Konchakovski, T. Steinert, W. Cassing, E.L. Bratkovskaya, *Phys. Rev. C* **92**(5), 054914 (2015). DOI 10.1103/PhysRevC.92.054914
57. M. Greif, F. Senzel, H. Kremer, K. Zhou, C. Greiner, Z. Xu, *Phys. Rev. C* **95**(5), 054903 (2017). DOI 10.1103/PhysRevC.95.054903
58. V. Vovchenko, L.G. Pang, H. Niemi, I.A. Karpenko, M.I. Gorenstein, L.M. Satarov, I.N. Mishustin, B. Kämpfer, H. Stoecker, *PoS BORMIO2016*, 039 (2016). DOI 10.22323/1.272.0039

59. J. Berges, K. Reygers, N. Tanji, R. Venugopalan, Nucl. Phys. A **967**, 708 (2017). DOI 10.1016/j.nuclphysa.2017.04.034
60. L. Oliva, M. Ruggieri, S. Plumari, F. Scardina, G.X. Peng, V. Greco, Phys. Rev. C **96**(1), 014914 (2017). DOI 10.1103/PhysRevC.96.014914
61. O. Garcia-Montero, A. Mazeliauskas, P. Plaschke, S. Schlichting, JHEP **03**, 053 (2024). DOI 10.1007/JHEP03(2024)053
62. J. Cleymans, V.V. Goloviznin, K. Redlich, Phys. Rev. D **47**, 173 (1993). DOI 10.1103/PhysRevD.47.173
63. A. Kurkela, A. Mazeliauskas, J.F. Paquet, S. Schlichting, D. Teaney, Phys. Rev. C **99**(3), 034910 (2019). DOI 10.1103/PhysRevC.99.034910
64. A. Kurkela, A. Mazeliauskas, J.F. Paquet, S. Schlichting, D. Teaney, Phys. Rev. Lett. **122**(12), 122302 (2019). DOI 10.1103/PhysRevLett.122.122302
65. P.B. Arnold, G.D. Moore, L.G. Yaffe, JHEP **01**, 030 (2003). DOI 10.1088/1126-6708/2003/01/030
66. C. Gale, J.F. Paquet, B. Schenke, C. Shen, Phys. Rev. C **105**(1), 014909 (2022). DOI 10.1103/PhysRevC.105.014909
67. A. Bazavov, T. Bhattacharya, C. DeTar, H.T. Ding, S. Gottlieb, R. Gupta, P. Hegde, U. Heller, F. Karsch, E. Laermann, L. Levkova, S. Mukherjee, P. Petreczky, C. Schmidt, C. Schroeder, R. Soltz, W. Soeldner, R. Sugar, M. Wagner, P. Vranas, Physical Review D **90**(9) (2014). DOI 10.1103/physrevd.90.094503. URL <http://dx.doi.org/10.1103/PhysRevD.90.094503>
68. B. Schenke, P. Tribedy, R. Venugopalan, Phys. Rev. Lett. **108**, 252301 (2012). DOI 10.1103/PhysRevLett.108.252301
69. D. Everett, et al., Phys. Rev. Lett. **126**(24), 242301 (2021). DOI 10.1103/PhysRevLett.126.242301
70. G. Nijs, W. van der Schee, U. Gürsoy, R. Snellings, Phys. Rev. C **103**(5), 054909 (2021). DOI 10.1103/PhysRevC.103.054909
71. M.R. Heffernan, C. Gale, S. Jeon, J.F. Paquet, Phys. Rev. Lett. **132**(25), 252301 (2024). DOI 10.1103/PhysRevLett.132.252301
72. M.M. Aggarwal, et al., Phys. Rev. C **58**, 1146 (1998). DOI 10.1103/PhysRevC.58.1146
73. M.M. Aggarwal, et al., Phys. Lett. B **458**, 422 (1999). DOI 10.1016/S0370-2693(99)00560-2
74. L.J. Johnson, Nucl. Phys. A **715**, 691 (2003). DOI 10.1016/S0375-9474(02)01468-9
75. K. Reygers, Nucl. Phys. A **715**, 683 (2003). DOI 10.1016/S0375-9474(02)01466-5
76. M. Wilde, Nucl. Phys. A **904-905**, 573c (2013). DOI 10.1016/j.nuclphysa.2013.02.079
77. N. Götz, A. Schäfer, O. Garcia-Montero, J.F. Paquet, H. Elfner, C. Gale, Phys. Rev. C **105**(4), 044910 (2022). DOI 10.1103/PhysRevC.105.044910. [Erratum: Phys.Rev.C 109, 049901 (2024)]
78. A. Adare, et al., Phys. Rev. C **91**(6), 064904 (2015). DOI 10.1103/PhysRevC.91.064904
79. L. Adamczyk, et al., Phys. Lett. B **770**, 451 (2017). DOI 10.1016/j.physletb.2017.04.050
80. J. Adam, et al., Phys. Lett. B **754**, 235 (2016). DOI 10.1016/j.physletb.2016.01.020
81. G. David, Rept. Prog. Phys. **83**(4), 046301 (2020). DOI 10.1088/1361-6633/ab6f57
82. K. Reygers, Acta Phys. Polon. Supp. **16**(1), 1 (2023). DOI 10.5506/APhysPolBSupp.16.1-A19
83. R. Chatterjee, E.S. Frodermann, U.W. Heinz, D.K. Srivastava, Phys. Rev. Lett. **96**, 202302 (2006). DOI 10.1103/PhysRevLett.96.202302
84. A. Adare, et al., Phys. Rev. C **94**(6), 064901 (2016). DOI 10.1103/PhysRevC.94.064901
85. S. Acharya, et al., Phys. Lett. B **789**, 308 (2019). DOI 10.1016/j.physletb.2018.11.039
86. H. van Hees, M. He, R. Rapp, Nucl. Phys. A **933**, 256 (2015). DOI 10.1016/j.nuclphysa.2014.09.009
87. C. Gale, Y. Hidaka, S. Jeon, S. Lin, J.F. Paquet, R.D. Pisarski, D. Satow, V.V. Skokov, G. Vujanovic, Phys. Rev. Lett. **114**, 072301 (2015). DOI 10.1103/PhysRevLett.114.072301
88. Y.M. Kim, C.H. Lee, D. Teaney, I. Zahed, Phys. Rev. C **96**(1), 015201 (2017). DOI 10.1103/PhysRevC.96.015201
89. V. Skokov, A.Y. Illarionov, V. Toneev, Int. J. Mod. Phys. A **24**, 5925 (2009). DOI 10.1142/S0217751X09047570

90. K. Tuchin, Phys. Rev. C **93**(1), 014905 (2016). DOI 10.1103/PhysRevC.93.014905
91. X.G. Huang, Rept. Prog. Phys. **79**(7), 076302 (2016). DOI 10.1088/0034-4885/79/7/076302
92. P. Adhikari, et al., (2024)
93. L. McLerran, V. Skokov, Nucl. Phys. A **929**, 184 (2014). DOI 10.1016/j.nuclphysa.2014.05.008
94. G. Basar, D. Kharzeev, D. Kharzeev, V. Skokov, Phys. Rev. Lett. **109**, 202303 (2012). DOI 10.1103/PhysRevLett.109.202303
95. B. Muller, S.Y. Wu, D.L. Yang, Phys. Rev. D **89**(2), 026013 (2014). DOI 10.1103/PhysRevD.89.026013
96. X. Wang, I.A. Shovkovy, L. Yu, M. Huang, Phys. Rev. D **102**(7), 076010 (2020). DOI 10.1103/PhysRevD.102.076010
97. A. Ayala, J.D. Castano-Yepes, C.A. Dominguez, L.A. Hernandez, S. Hernandez-Ortiz, M.E. Tejeda-Yeomans, Phys. Rev. D **96**(1), 014023 (2017). DOI 10.1103/PhysRevD.96.014023. [Erratum: Phys.Rev.D 96, 119901 (2017)]
98. J.A. Sun, L. Yan, Phys. Rev. C **109**(3), 034917 (2024). DOI 10.1103/PhysRevC.109.034917
99. M. Mayer, A. Dash, G. Inghirami, H. Elfner, L. Rezzolla, D.H. Rischke, (2024)
100. M. Mayer, A. Dash, G. Inghirami, H. Elfner, L. Rezzolla, D.H. Rischke, (2024)
101. R. Baier, B. Pire, D. Schiff, Phys. Rev. D **38**, 2814 (1988). DOI 10.1103/PhysRevD.38.2814
102. T. Altherr, P. Aurenche, Z. Phys. C **45**, 99 (1989). DOI 10.1007/BF01556676
103. P. Aurenche, F. Gelis, G.D. Moore, H. Zaraket, JHEP **12**, 006 (2002). DOI 10.1088/1126-6708/2002/12/006
104. M. Laine, JHEP **11**, 120 (2013). DOI 10.1007/JHEP11(2013)120
105. G. Vujanovic, J.F. Paquet, G.S. Denicol, M. Luzum, S. Jeon, C. Gale, Phys. Rev. C **94**(1), 014904 (2016). DOI 10.1103/PhysRevC.94.014904
106. G. Vujanovic, G.S. Denicol, M. Luzum, S. Jeon, C. Gale, Phys. Rev. C **98**(1), 014902 (2018). DOI 10.1103/PhysRevC.98.014902
107. G. Vujanovic, J.F. Paquet, C. Shen, G.S. Denicol, S. Jeon, C. Gale, U. Heinz, Phys. Rev. C **101**, 044904 (2020). DOI 10.1103/PhysRevC.101.044904
108. R. Rapp, PoS **CPOD2009**, 040 (2009). DOI 10.22323/1.071.0040
109. J. Churchill, L. Du, C. Gale, G. Jackson, S. Jeon, Phys. Rev. C **109**(4), 044915 (2024). DOI 10.1103/PhysRevC.109.044915
110. H. Gervais, S. Jeon, Phys. Rev. C **86**, 034904 (2012). DOI 10.1103/PhysRevC.86.034904
111. T. Sjostrand, S. Mrenna, P.Z. Skands, JHEP **05**, 026 (2006). DOI 10.1088/1126-6708/2006/05/026
112. S. Camarda, et al., Eur. Phys. J. C **80**(3), 251 (2020). DOI 10.1140/epjc/s10052-020-7757-5. [Erratum: Eur.Phys.J.C 80, 440 (2020)]
113. H. van Hees, C. Gale, R. Rapp, Phys. Rev. C **84**, 054906 (2011). DOI 10.1103/PhysRevC.84.054906
114. C. Shen, U.W. Heinz, J.F. Paquet, C. Gale, Phys. Rev. C **89**(4), 044910 (2014). DOI 10.1103/PhysRevC.89.044910
115. O. Massen, G. Nijts, M. Sas, W. van der Schee, R. Snellings, (2024)
116. R.J. Porter, et al., Phys. Rev. Lett. **79**, 1229 (1997). DOI 10.1103/PhysRevLett.79.1229
117. H.J. Specht, Nucl. Phys. A **805**, 338 (2008). DOI 10.1016/j.nuclphysa.2008.02.275
118. R. Arnaldi, et al., Eur. Phys. J. C **61**, 711 (2009). DOI 10.1140/epjc/s10052-009-0878-5
119. F. Geurts, Nucl. Phys. A **904-905**, 217c (2013). DOI 10.1016/j.nuclphysa.2013.01.062
120. K. Ozawa, et al., Eur. Phys. J. C **43**, 421 (2005). DOI 10.1140/epjc/s2005-02212-3
121. V.J.G. Feuillard, PoS **PANIC2021**, 233 (2022). DOI 10.22323/1.380.0233
122. C. Jin. *Hard Probes 2024* (2024)
123. P. Huck, Nucl. Phys. A **931**, 659 (2014). DOI 10.1016/j.nuclphysa.2014.09.090
124. F. Geurts, R.A. Tripolt, Prog. Part. Nucl. Phys. **128**, 104004 (2023). DOI 10.1016/j.pnpnp.2022.104004
125. J.I. Kapusta, E.V. Shuryak, Phys. Rev. D **49**, 4694 (1994). DOI 10.1103/PhysRevD.49.4694
126. P.M. Hohler, R. Rapp, Phys. Lett. B **731**, 103 (2014). DOI 10.1016/j.physletb.2014.02.021
127. C. Ahdida, et al. Letter of Intent: the NA60+ experiment (2022)

128. R. Rapp, H. van Hees, Phys. Lett. B **753**, 586 (2016). DOI 10.1016/j.physletb.2015.12.065
129. STAR. Temperature Measurement of Quark-Gluon Plasma at Different Stages (2024)
130. J. Churchill, L. Du, C. Gale, G. Jackson, S. Jeon, Phys. Rev. Lett. **132**(17), 172301 (2024). DOI 10.1103/PhysRevLett.132.172301
131. S.M.H. Wong, Z. Phys. C **53**, 465 (1992). DOI 10.1007/BF01625907
132. B.S. Kasmaei, M. Strickland, Phys. Rev. D **99**(3), 034015 (2019). DOI 10.1103/PhysRevD.99.034015
133. M. Martinez, M. Strickland, Phys. Rev. C **78**, 034917 (2008). DOI 10.1103/PhysRevC.78.034917
134. M. Coquet, X. Du, J.Y. Ollitrault, S. Schlichting, M. Winn, Phys. Lett. B **821**, 136626 (2021). DOI 10.1016/j.physletb.2021.136626
135. O. Garcia-Montero, P. Plaschke, S. Schlichting, (2024)
136. X.Y. Wu, L. Du, C. Gale, S. Jeon, Phys. Rev. C **110**(5), 054904 (2024). DOI 10.1103/PhysRevC.110.054904
137. J.F. Paquet. Conference Highlights: Electroweak Probes, *Hard Probes 2024*, and private communication (2024)
138. P. Steinbrecher, Nucl. Phys. A **982**, 847 (2019). DOI 10.1016/j.nuclphysa.2018.08.025
139. R. Chatterjee, D.K. Srivastava, U.W. Heinz, C. Gale, Phys. Rev. C **75**, 054909 (2007). DOI 10.1103/PhysRevC.75.054909
140. F. Geurts, J. Phys. Conf. Ser. **458**, 012016 (2013). DOI 10.1088/1742-6596/458/1/012016
141. E. Speranza, Virtual photon polarization and dilepton anisotropy in pion-nucleon and heavy-ion collisions. Ph.D. thesis, Darmstadt, Tech. U. (2018). DOI 10.15120/GSI-2018-01176
142. F. Seck, B. Friman, T. Galatyuk, H. van Hees, R. Rapp, E. Speranza, J. Wambach, Phys. Lett. B **861**, 139267 (2025). DOI 10.1016/j.physletb.2025.139267
143. R. Arnaldi, et al., Phys. Rev. Lett. **102**, 222301 (2009). DOI 10.1103/PhysRevLett.102.222301
144. G. Baym, T. Hatsuda, M. Strickland, Phys. Rev. C **95**(4), 044907 (2017). DOI 10.1103/PhysRevC.95.044907
145. M. Coquet, M. Winn, X. Du, J.Y. Ollitrault, S. Schlichting, Phys. Rev. Lett. **132**(23), 232301 (2024). DOI 10.1103/PhysRevLett.132.232301
146. S. Hauksson, C. Gale, Phys. Rev. C **109**(3), 034902 (2024). DOI 10.1103/PhysRevC.109.034902
147. X.Y. Wu, H. Gao, B. Forster, C. Gale, G. Jackson, S. Jeon, (2024)
148. D. Kumar Srivastava, C. Gale, Phys. Lett. B **319**, 407 (1993). DOI 10.1016/0370-2693(93)91742-6
149. O. Garcia-Montero, N. Löhner, A. Mazeliauskas, J. Berges, K. Reygers, Phys. Rev. C **102**(2), 024915 (2020). DOI 10.1103/PhysRevC.102.024915
150. C. Shen, J.F. Paquet, G.S. Denicol, S. Jeon, C. Gale, Phys. Rev. C **95**(1), 014906 (2017). DOI 10.1103/PhysRevC.95.014906
151. D.K. Srivastava, C. Gale, R.J. Fries, Phys. Rev. C **67**, 034903 (2003). DOI 10.1103/PhysRevC.67.034903
152. R.M. Yazdi, S. Shi, C. Gale, S. Jeon, Acta Phys. Polon. Supp. **16**(1), 1 (2023). DOI 10.5506/APhysPolBSupp.16.1-A129
153. R. Bailhache, et al., Phys. Rept. **1097**, 1 (2024). DOI 10.1016/j.physrep.2024.10.002